INTERNATIONAL JOURNAL OF ENERGY RESEARCH, VOL. 17, 000–000 (1993)

HEAT AND FLUID TRANSPORT IN AN EVAPORATIVE CAPILLARY PUMP

H. G. WULZ

Department of Space Thermal Technologies, Dornier GmbH, Postbox 14 20, D-7990 Friedrichshafen, Germany

AND

F. MAYINGER

Department of Thermodynamics A, Technical University of Munich, Arcisstraße 21, D-8000 München 2, Germany

SUMMARY

The thermal and fluid mechanical properties of an evaporative capillary pump are described by means of characteristics that have been determined by tests. The capillary pump, which has been newly designed for an applic[max]ation in future space projects, serves a double function as the heat absorbing element in a closed loop as well as a pump circulating the working fluid. The working fluids used were CCl_3F (freon R11) and liquid anhydrous ammonia. The paper describes the associated heat and mass transport in the capillary pump, and the physical process of the capillary pumping is explained. Furthermore, a model is introduced which explains the boiling heat transfer in the porous structure of the capillary pump.

INTRODUCTION

Task of capillary pump

The evaporative capillary pump described in this paper has been newly developed in the frame of a technology project that has been sponsored by the German Ministry of Research and Development. Capillary pumped loops (CPL) are the most promising new technical concepts for the active thermal control of future large satellites and unmanned space platforms that have to meet the strict requirements of noiseless and vibrationless operation. The essential advantages that one expects from these novel heat transport systems for space vehicles have been described [1–3].

In Figure 1, the working principle of a simple capillary pumped loop is explained. The capillary pump (1) contains a porous wick structure (2) in which the subcooled working fluid is stored. Heat, which is produced by a heat generating equipment, or by a container to be cooled, flows to the surface of the porous wick (3) where the working fluid evaporates. The vapour flows through the vapour line (4) and transports the heat to the heat sink, i.e. a condensing heat exchanger, or, briefly, a condenser (5). There the vapour condenses, and the heat of condensation is rejected to the ambience. The subcooled working fluid travels back through the liquid return line (6) and enters the wick again.

In principle, several working fluids commonly used in the refrigeration industry can be applied in CPLs. During the development of the capillary pump, such working fluids as fluorochlorine-hydrocarbons (freons), water and liquid ammonia were used. The last was the preferred fluid with regard to the relatively high latent heat of evaporation and to the suitable boiling pressure at working temperature.

A patent has been granted [4, 5] for this capillary pump design.

0363–907X/93/000000–00$05.00

Received 12 March 1992
Revised 3 June 1992

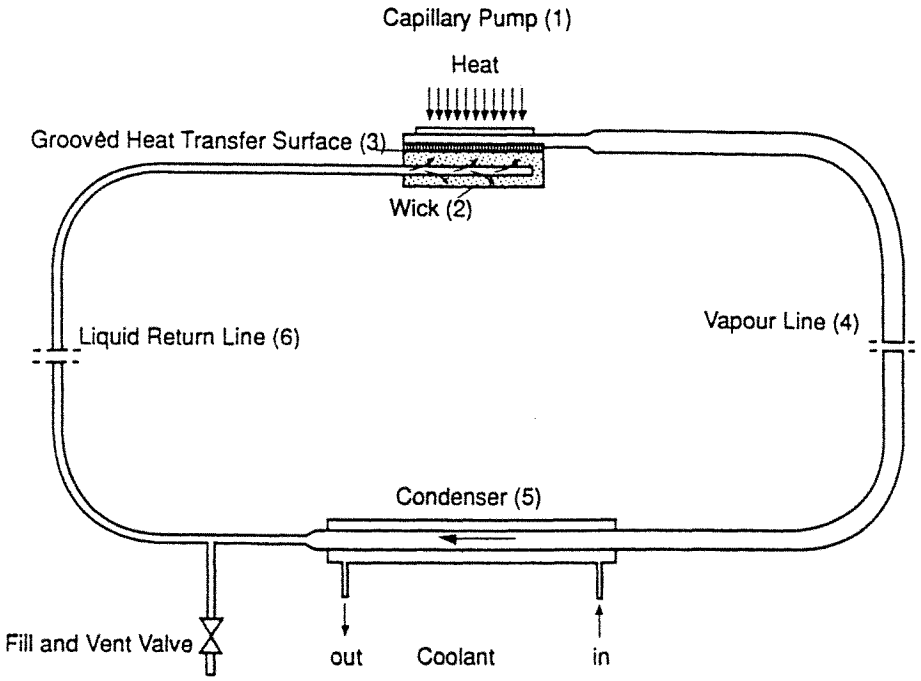

Figure 1. Working principle of capillary pumped loop

DESCRIPTION OF CAPILLARY-PUMP DESIGN

Working principle

The parts of the capillary pump are shown in Figure 2 and 3. The capillary pump basically consists of a flat porous wick, the base plate, in which the wick is embedded, and the cover plate.

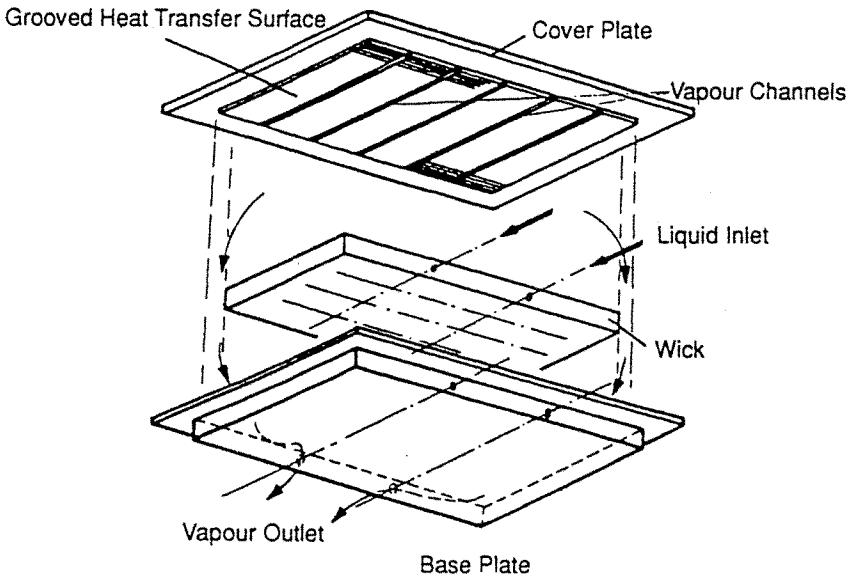

Figure 2. Schematic diagram of evaporative capillary pump using flat wick structure

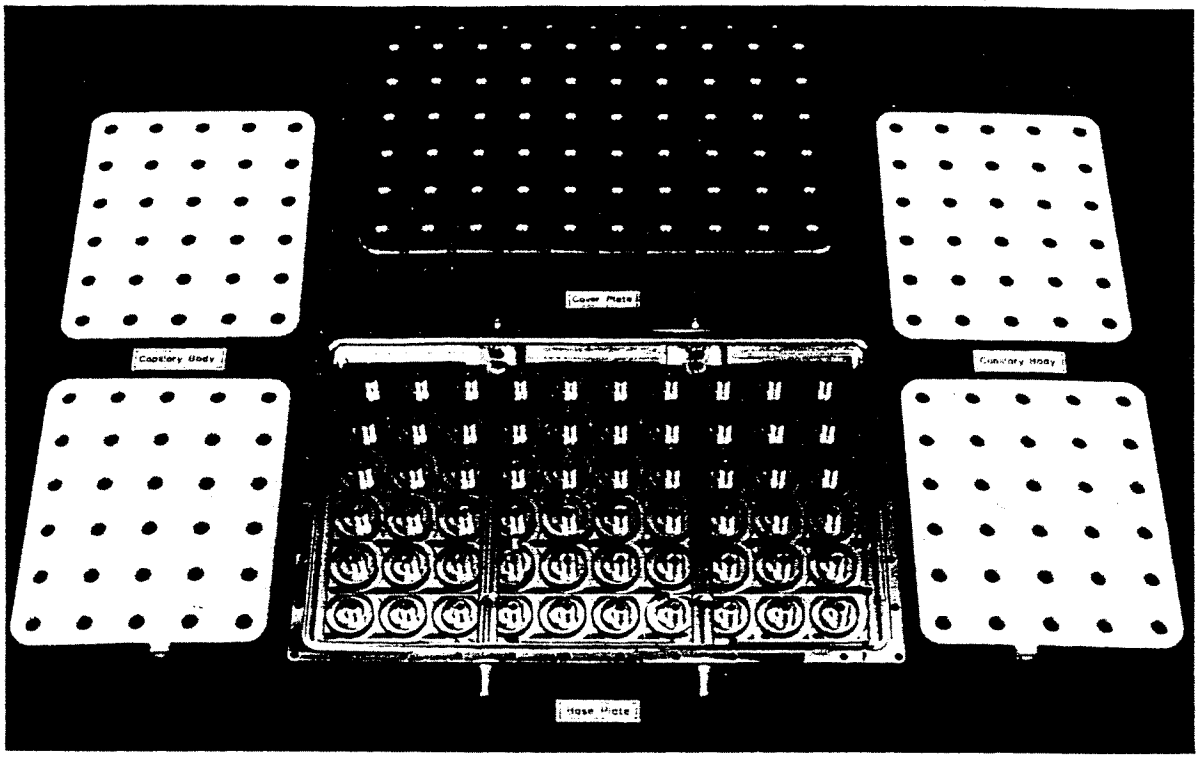

Figure 3. Ammonia capillary pump with wick assembly

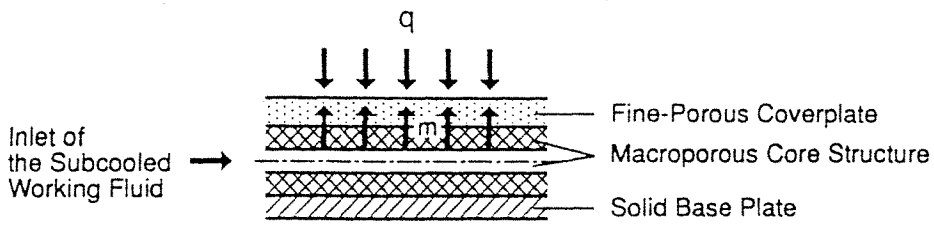

Figure 4. Schematic diagram of wick assembly

The wick structure is built up of several parts, as shown in Figure 4. It consists of a macroporous core structure of porous polyethylene which stores the subcooled working fluid. The liquid working fluid is distributed by a channel system which is drilled into the porous core structure as shown in Figure 5. The core structure is embedded in a machined base plate of polytetrafluoroethylene (Teflon) solid material.

On the heat input side, the fine porous top plate is pressed against the core structure. The top plate of the wick assembly is made of fine porous Teflon which exhibits an isotropic and homogeneous capillary structure. The relative pore volume, which is experimentally determined by mercury porosimetry and the cumulative pore volume depending on the pore radius r_p, is shown in Figure 6. One can see a pore maximum at a pore radius of about $r_p = 10\ \mu m$, which is widened unsymmetrically on the side of decreasing values of the pore radius. A qualitative comparison of this pore profile with that of packed spheres leads to the assumption that the physical structure of the fine porous wick material can be well characterized by the model of packed spheres.

The evaporation of the working fluid takes place in a thin surface layer of the fine porous top plate, called the 'vapour zone'. The evaporated molecules are replaced by capillary forces at the liquid–vapour interface.

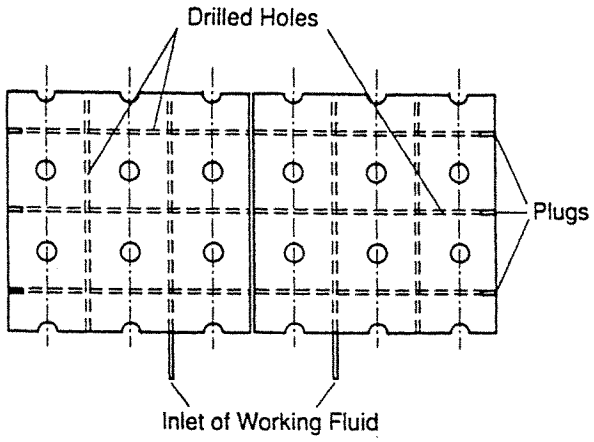

Figure 5. Distribution of subcooled working fluid in macroporous core structure of wick assembly

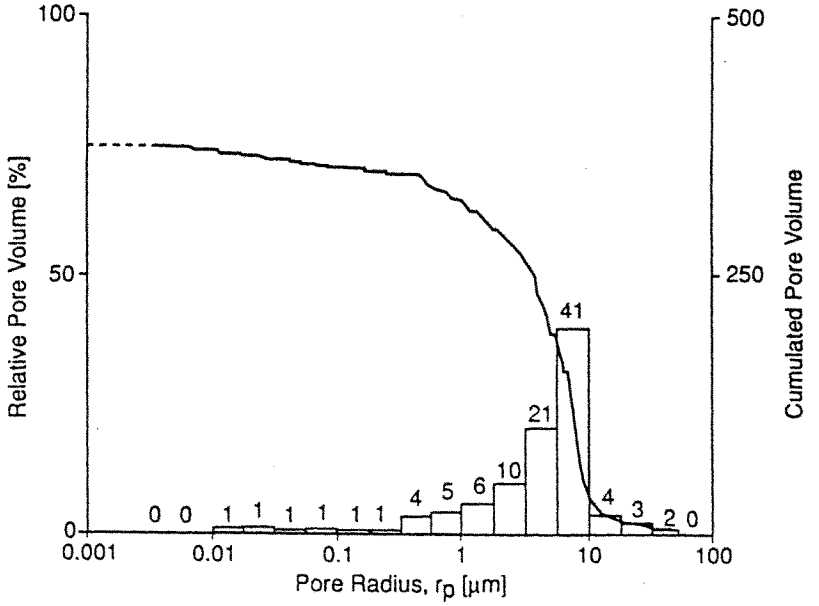

Figure 6. Pore profile of top plate of wick assembly made of fine porous TFE (Teflon)

In this way, a fluid transport is induced by capillary action. The process of capillary pumping is described in later in the paper.

The base plate of the capillary pump is shown in Figure 3. It is made in the same way as the cover plate, of aluminium alloy 6061. The cover plate and the base plate are connected by hollow bolts, which are arranged in a square pattern, to absorb the boiling pressure forces of the working fluid.

The bottom side of the cover plate shows a fine-grooved heat-transfer surface. In an orthogonal direction, vapour-collecting channels are milled equidistantly to collect the vapour fluxes leaving the grooves and to guide them to the outlet port, located at the sidewall of the capillary pump.

TEST SET-UP

The characteristics of the capillary pump were determined on a test loop, which is depicted in Figure 8. In addition to the capillary pump (1) the loop is built up of the condenser (2), the storage vessel (5), the vapour line and the liquid line (4). The condenser has been designed as a double-tube heat exchanger which is passed

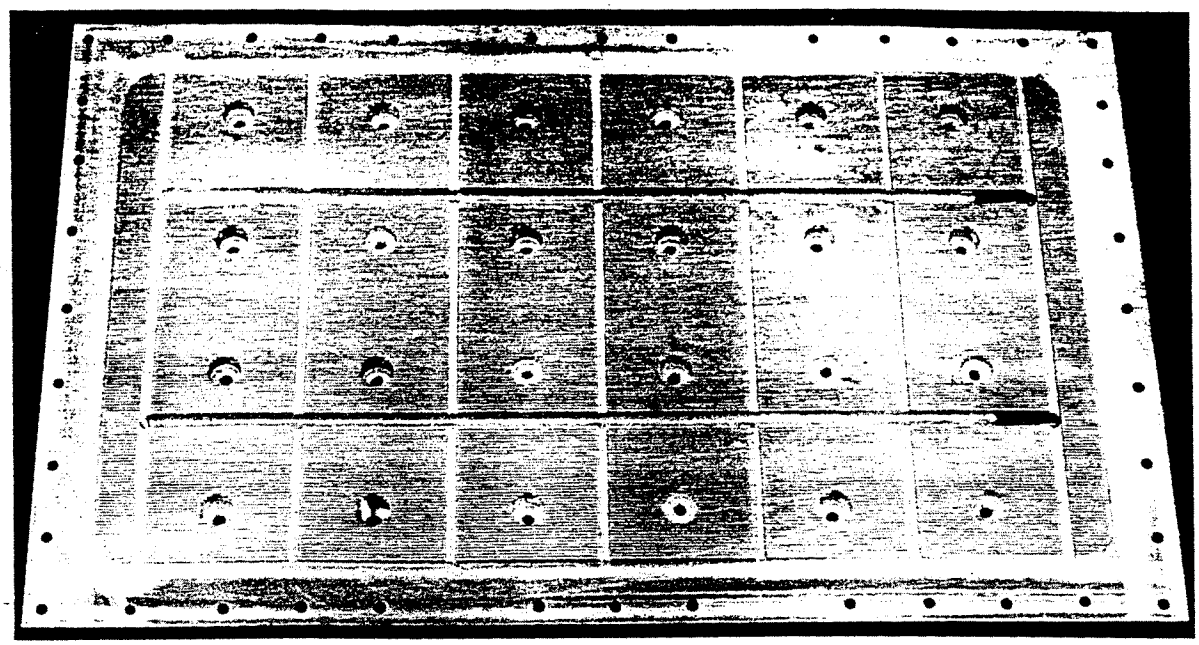

Figure 7. Cover plate of capillary pump tested with R11: view on grooved heat transfer area milled at bottom side

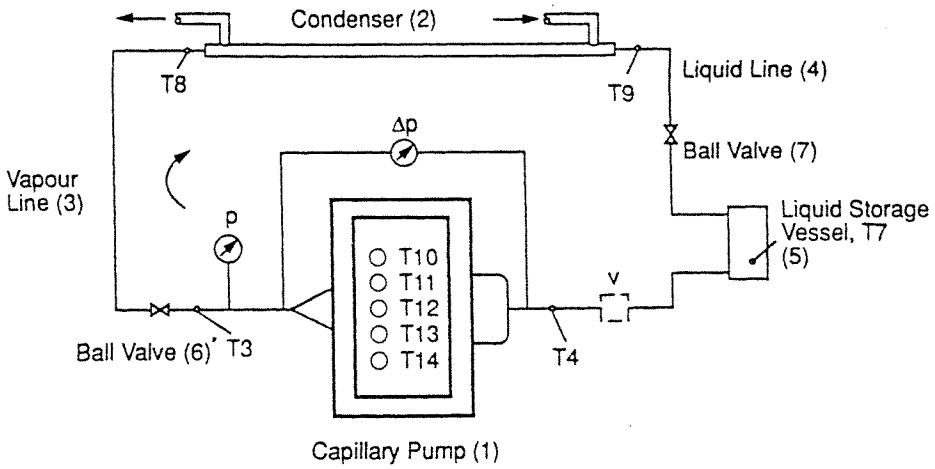

Figure 8. Schematic diagram of test loop, indicating positions of temperature and pressure measuring points

by the coolant methanol in the counter flow mode. The ball valve (6), which is mounted in the vapour line, is provided in order to vary the pressure drop of the loop for the determination of the pump characteristics of the capillary pump. The working fluids used were anhydrous ammonia with a purity grade of 99·95% and freon R11.

CHARACTERISTICS OF CAPILLARY PUMP

Effective capillary pumping pressure Δp_{eff} and heat transfer coefficient h

The temperature is the essential physical variable of the capillary pump and of the loop. The capillary pump responds to a variation of the heat flux determined by temperatures changes which are measured at different

points of its surface and in the vapour outlet port. From the temperatures, the heat transfer coefficient h is calculated as

$$h = \frac{q}{\Delta T} \tag{1}$$

q denotes the heat flux density, and ΔT is the difference between the average temperature T_{av} of the heat input surface of the capillary pump and the vapour temperature T_v:

$$\Delta T = T_{av} - T_v \tag{2}$$

The second important variable is the pressure drop Δp_{loop} of the loop, which is measured between the liquid inlet port and the vapour outlet port of the capillary pump. This pressure drop has to be overcome by the effective capillary pumping pressure Δp_{eff} generated by the capillary pump. In the steady-state working range $Q_{min} \leqslant Q < Q_{dry}$, the capillary pumping pressure and the pressure drop of the loop are in equilibrium:

$$\Delta p_{eff} = \Delta p_{loop} \tag{3}$$

Q_{min} denotes the minimum heat flux which is required for a stationary and continuous circulation of the working fluid in the loop. Q_{dry} is the critical heat flux which leads to a dry-out of the capillary pump.

If h and Δp_{eff} are plotted against the applied heat flux Q, one obtains the characteristics of the capillary pump, $h = h(Q)$ and $\Delta p_{eff} = \Delta p_{eff}(Q)$, respectively. These curves characterize the thermal and fluid mechanical properties of the capillary pump in its function as a heat absorbing element and as a circulation pump, respectively. Since there is a functional dependency of the applied heat flux $\dot{Q}$, and the mass flow m, see equation (4), Δp_{eff} is also plotted in the diagram against m, $\Delta p_{eff} = \Delta p_{eff}(m)$.

The mass flow is determined by calculation ((equation (4)) as a consequence of the proportionality of the heat and the fluid flow,

$$m = \frac{Q}{\Delta h_{1,v} + c_{p,f}(T_{sat} - T_{subcool})} \simeq \frac{Q}{\Delta h_{1,v}} \tag{4}$$

The heat which is required to heat the subcooled working fluid to the saturation temperature, i.e. $c_{p,f}\,(T_{sat} - T_{subcool})$, amounts at most to 1% of the latent heat of evaporation $\Delta h_{1,v}$, depending on the working fluids used, and therefore it is neglected.

Pump characteristic and flow resistance characteristic of loop

In Figure 9, the performance map of a capillary pump which has been tested with the working fluid CCl_3F (freon R11) is presented. Figure 10 shows the performance map of a capillary pump operated with ammonia. On plotting the loop pressure drop, Δp_{loop} against the applied heat flux Q, one obtains the flow resistance characteristic of the loop. Since, in the steady-state working range $Q_{min} \leqslant Q < Q_{dry}$, the effective capillary pumping pressure and the pressure drop of the loop are in equilibrium, both curves, the pump characteristic and the flow resistance characteristic of the loop, are identical. The curves, which were presented as thin lines in Figures 9 and 10, were obtained in tests in which the pressure drop of the loop was increased by the shutting of the ball valve in steps of α_i, where $i = 0,1,2,3, \ldots$

At this point, it should be noted that no analogy exists to the characteristics of a turbomachine. For the example of a centrifugal pump, two independent variables are selected. They are usually the pump speed and the volume flow. One obtains the associated pumping pressure from the point of intersection of a pump characteristic corresponding to a certain pump speed with the flow resistance curve of the loop. In contrast, the capillary pump possesses only one degree of freedom, i.e. the heat flux applied. Both the capillary pumping pressure and the mass flow change in response to the heat flux. The working points of the capillary pump move along the flow resistance curve of the loop if the heat flux is changed.

Pumping limit

The pumping limit of the capillary pump is characterized by the pumping limit curve. If a critical heat flux Q_{dry} is applied at a certain pressure drop, adjusted by the position of the ball valve, $\Delta p(\alpha_i)$, $i = 1,2,3, \ldots$, then

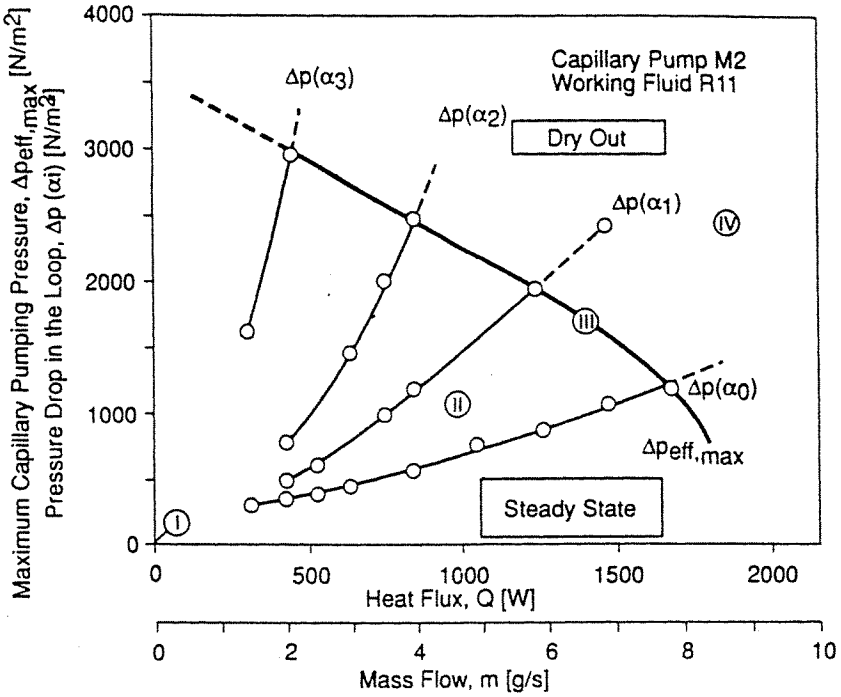

Figure 9. Performance diagram of capillary pump, working fluid R11: maximum effective available capillary pumping pressure, $\Delta p_{eff,max}$ *against applied heat flux* Q and against mass flow $m \rightarrow$ pumping limit curve (thick line): pressure loss in loop $\Delta p(\alpha_i)$ against applied heat flux Q and against mass flow $m \rightarrow$ pump characteristic/flow resistance characteristic (thin curves)

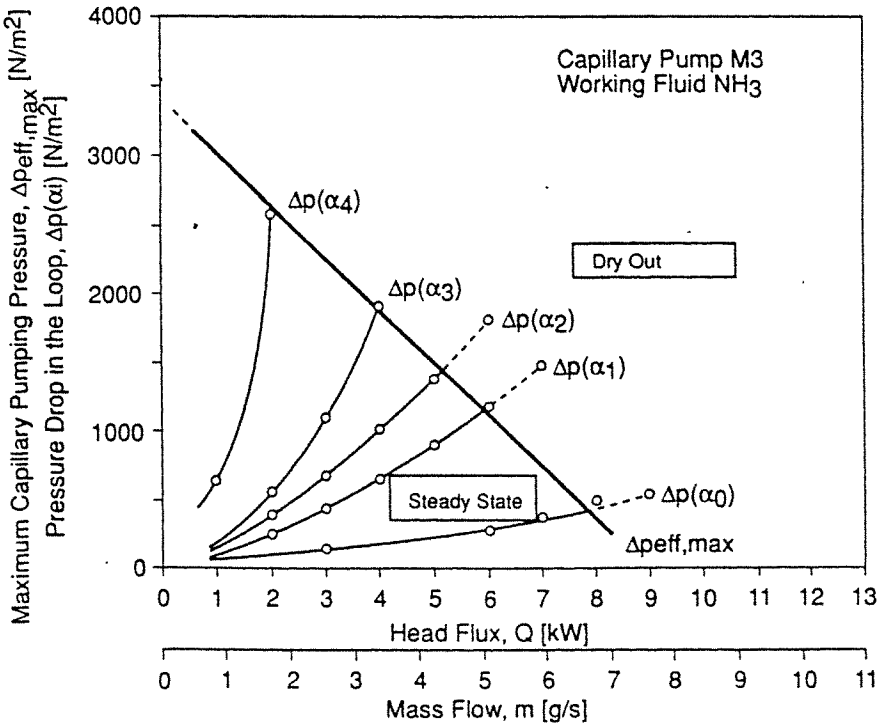

Figure 10. Performance diagram of ammonia capillary pump: maximum effective available capillary pumping pressure $\Delta p_{eff,max}$ against applied heat flux Q and against mass flow $m \rightarrow$ pumping limit curve; pressure loss in loop $\Delta p(\alpha_i)$ against applied heat flux Q and against mass flow $\rightarrow$ pump characteristic/flow resistance characteristic (thin curves)

the capillary pump begins to dry out. The critical working points in Figures 9 and 10 are connected by a thick line, labelled $\Delta p_{eff,max}$.

In the experiment, the dry out could be detected by monitoring the vapour temperature. In the steady-state working range the saturation temperature was always observed. If the dry-out state was reached, the temperature of the overheated vapour was regularly measured, $Q \gtrsim Q_{dry}$.

The pumping limit curve shows a monotonic decrease as the heat flux rises. It separates the steady-state working range, which extends below the curve, from the region where the capillary pump dries out. The slope of the graph is influenced by the internal pressure losses of the capillary pump. These losses depend on the design characteristics, e.g. the sizing of the grooved evaporation surface, the pore size of the wick etc. This is explained in more detail later in the paper. The intersection point of the pump characteristic with the pumping limit curve indicates the maximum heat flux Q_{max} which can be transported in the loop.

Heat transfer coefficient

The heat-transfer coefficient h of the capillary pump that was tested with CCl_3F (freon R11) is presented in Figure 11 as a function of the applied heat flux density q. The parameter is the pressure drop Δp which has been adjusted by the ball valve. The diagram shows a constant heat-transfer coefficient within the steady-state range, i.e. h is independent of the heat flux density. The dry out is indicated by a rapid descent of the graph. From this position, the graph is plotted as a dotted line. Figure 12 shows the heat-transfer coefficient of the capillary pump which was tested with ammonia. As a consequence of the better heat-transfer properties of ammonia (e.g. a high latent heat of evaporation) the corresponding heat-transfer coefficient is much higher than if freon were used.

Hydraulic power characteristic and hydraulic power limit curve of capillary pump

The hydraulic pumping power P_{hydr} of the capillary pump is calculated as follows:

$$P_{hydr} = \frac{m\Delta p(\alpha_i)}{\rho_f} \tag{5}$$

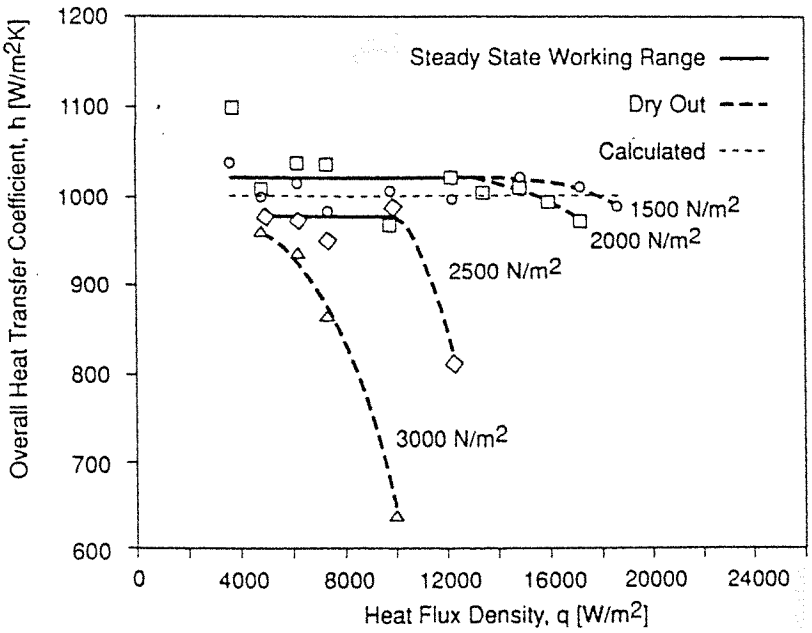

Figure 11. Overall heat transfer coefficient h of R11 capillary pump against applied heat flux density q: for comparison, thin dotted line is calculated value of h

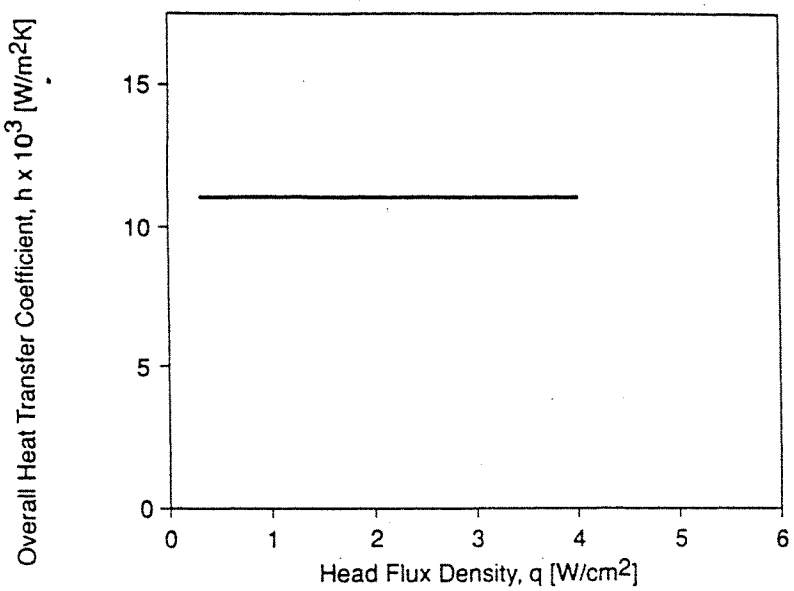

Figure 12. Overall heat transfer coefficient h of ammonia capillary pump against applied heat flux density q

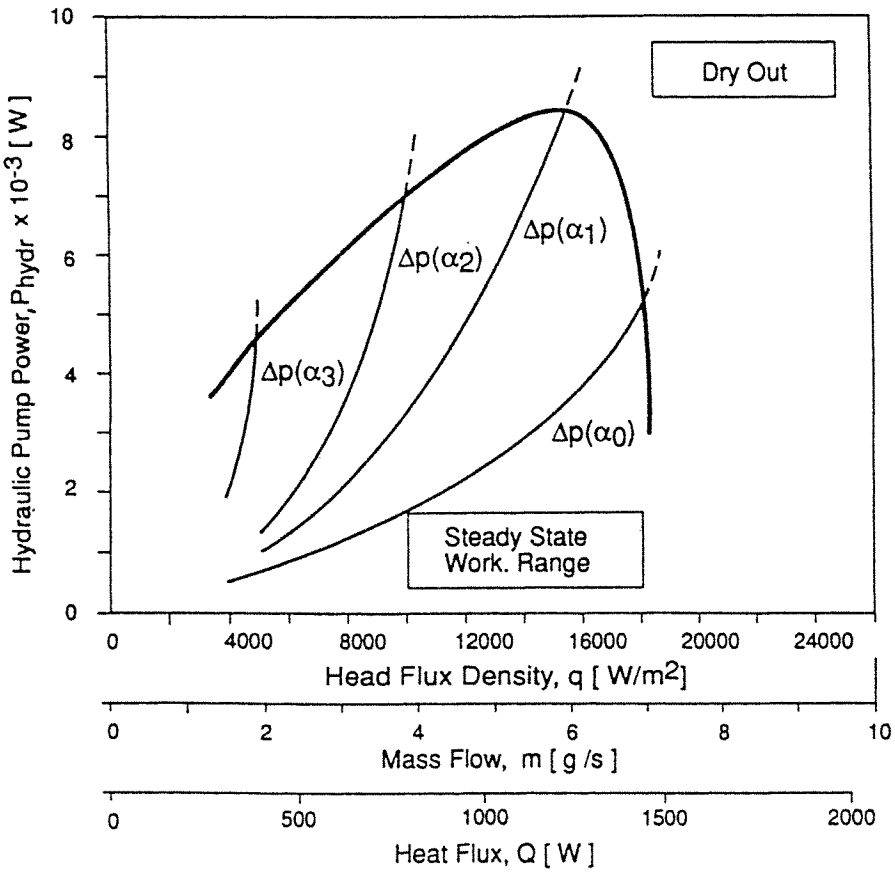

Figure 13. Hydraulic power characteristics (thin curves) and the hydraulic power limit curve (thick curve) of R11 capillary pump against heat flux density q, against mass flow m and against applied heat flux Q

where

$$m = \frac{Q}{\Delta h_{1,v}} = \text{mass flow} \tag{4a}$$

The curves that connect the pair of variables $[P_{hydr}; q]$ or $[P_{hydr}; m]$ or $[P_{hydr}; Q]$ are called the 'hydraulic power characteristics' of the capillary pump. They are plotted in Figure 13 for the capillary pump tested with R11. The parameter is the pressure drop $\Delta p(\alpha_i)$, which is adjusted by the ball valve. It can be noted that the hydraulic power for circulation of the working fluid is of the order of milliwatts. The thick line which connects the pair of variables $[P_{hydr}; Q_{dry}]$ or $[P_{hydr}; m_{dry}]$ or $[P_{hydr}; Q_{dry}]$ is called the 'hydraulic power limit curve'. It describes the maximum hydraulic power of the capillary pump in the steady-state working range.

MASS TRANSPORT EFFECTED BY CAPILLARY FORCES: CAPILLARY PUMPING PROCESS

Steps of heat and mass transport in capillary pump

The associated heat and mass transport in the capillary pump and the capillary pumping process have been studied in detail [6]. Figure 14 shows a cross-sectional sketch of the capillary pump. In section A, depicted in Figure 15, the individual partial steps of the heat and mass transfer can be seen.

For reasons of symmetry, the domain considered is limited by the centreline of a fin and the centreline of a groove. It is assumed that a proportional heat flux Q_{in} flows along the centreline of the fin to the surface of the porous wick. In the opposite direction a proportional mass flow—of the subcooled working fluid flows in the porous structure to the top of the fin. The working fluid evaporates in a thin vapour zone at the surface of the wick.

Partial steps of heat transfer: The heat transfer steps are

(*a*) conduction of the heat flux Q_{in} in the cover plate to the fins of the grooved surface
(*b*) transfer of the heat flux Q_{in} from the fins to the vapour zones of the wick structure; a partial flux Q_2 is transferred from the fin wall to the vapour produced and overheats it
(*c*) conduction of the heat flux $Q_1 = Q_{in} - Q_2$ in the vapour zone of the porous wick structure

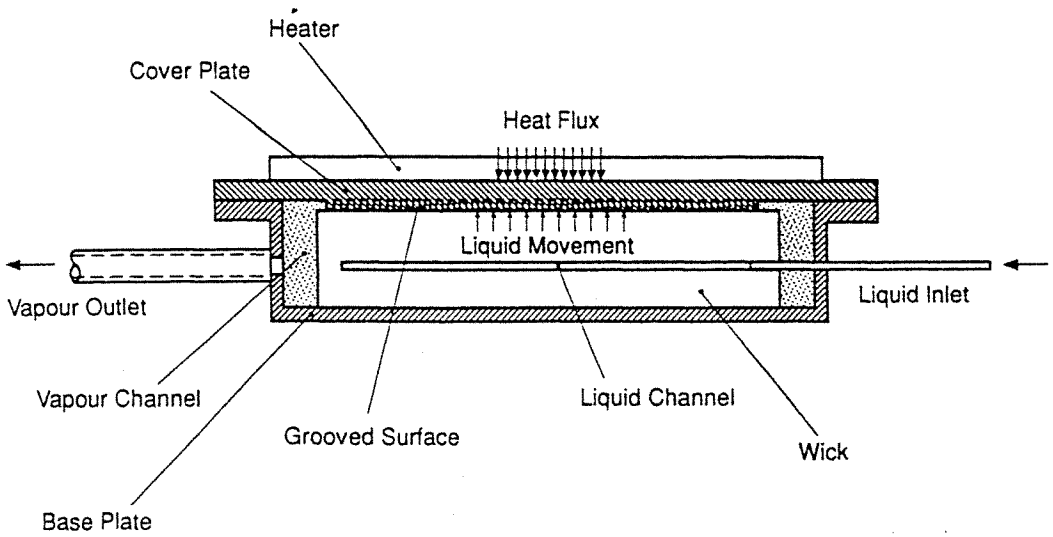

Figure 14. Cross-section of capillary pump with flat wick structure

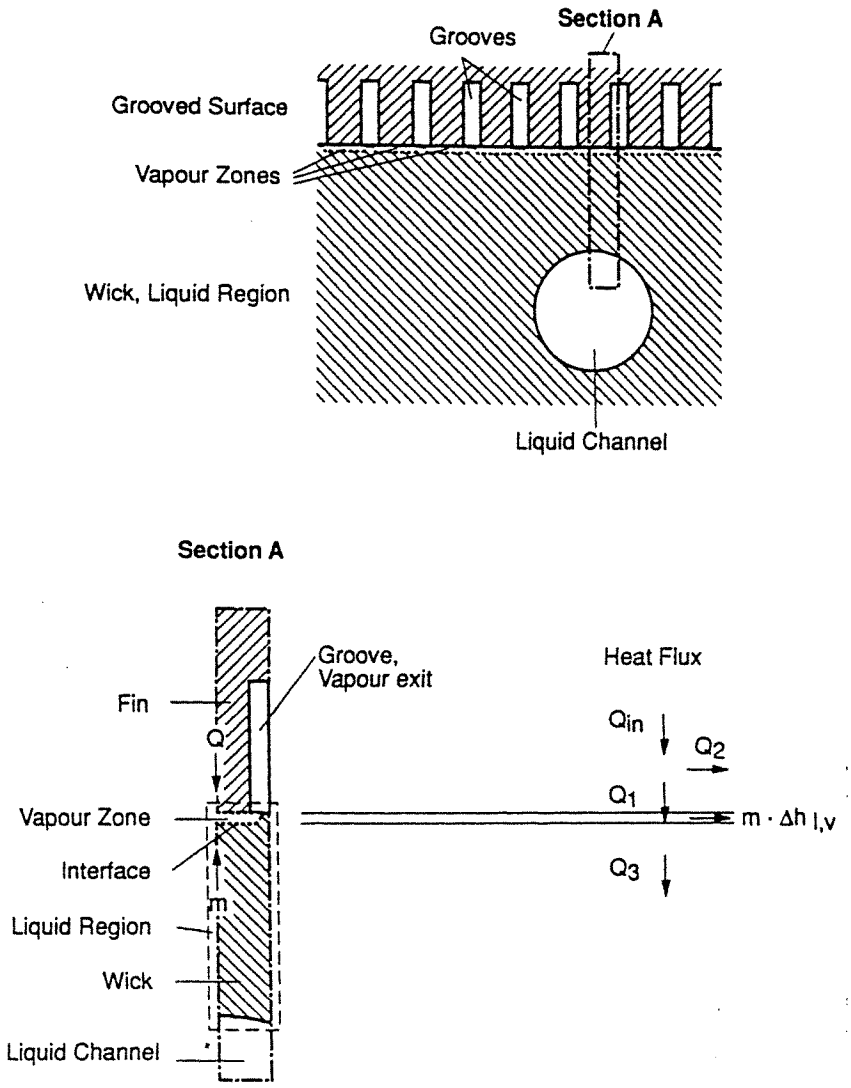

Figure 15. Heat and fluid transfer considered on model of a single fin

(*d*) transfer of the heat flux $Q_1 = m\Delta h_{1,v} + Q_3$ at the interface of the vapour zone to the boiling working fluid. The partial flux Q_3 flows into the liquid region of the wick structure and heats the subcooled liquid up to the saturation temperatures
(*e*) convective transport of the heat flux $m\Delta h_{1,v}$ by the vapour that flows off.

Partial steps of mass transfer: The mass transfer steps are

(*a*) flow of the subcooled working fluid in the feeder tubes of the evaporator and into the liquid channels of the wick structure
(*b*) entry of the subcooled working fluid into the pores of the wick structure
(*c*) laminar flow of the working fluid in the pore structure effected by capillary forces which act on the interface
(*d*) mass transfer of the boiling working fluid to the vapour phase at the interface
(*e*) vapour flow in the porous structure of the vapour zone
(*f*) vapour flow in the grooves and the vapour-collecting channels of the cover plate.

Physical process of capillary pumping

The physical process of capillary pumping is now explained by the use of simplified schematic model of a capillary pump of which the wick structure is idealized by packed spheres, see Figure 16. In proportion to the heat flux, some of the working fluid is transferred by evaporation from the phase boundary surface at position 0 to the vapour phase. The phase boundary surface in the wick structure is continuously renewed. Owing to the surface tension, new molecules are transported from the liquid pool stored in the wick to the phase boundary surface. As a consequence of continuity in the steady-state condition, the mass flow of the vapour leaving and the mass flow of the liquid entering the capillary pump are equal, i.e. $m_v = m_l$. In this way, a circulation takes place in the closed loop.

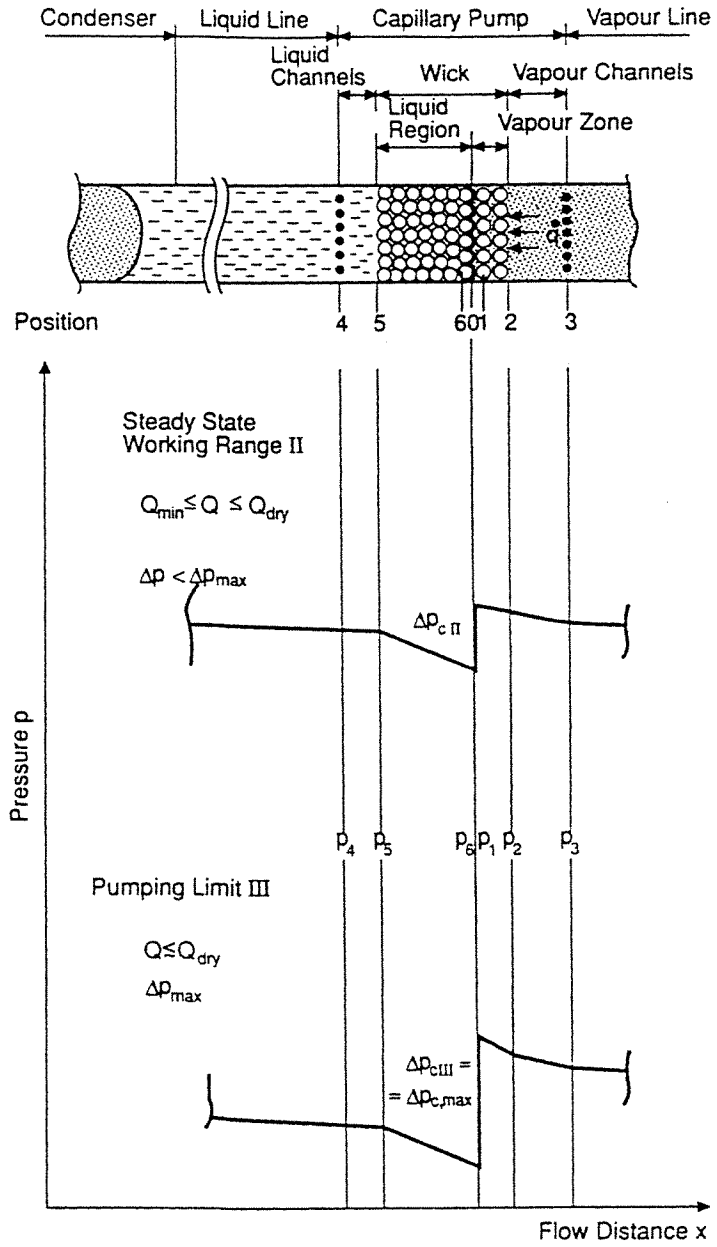

Figure 16. Schematic diagram showing pressure losses in capillary pump

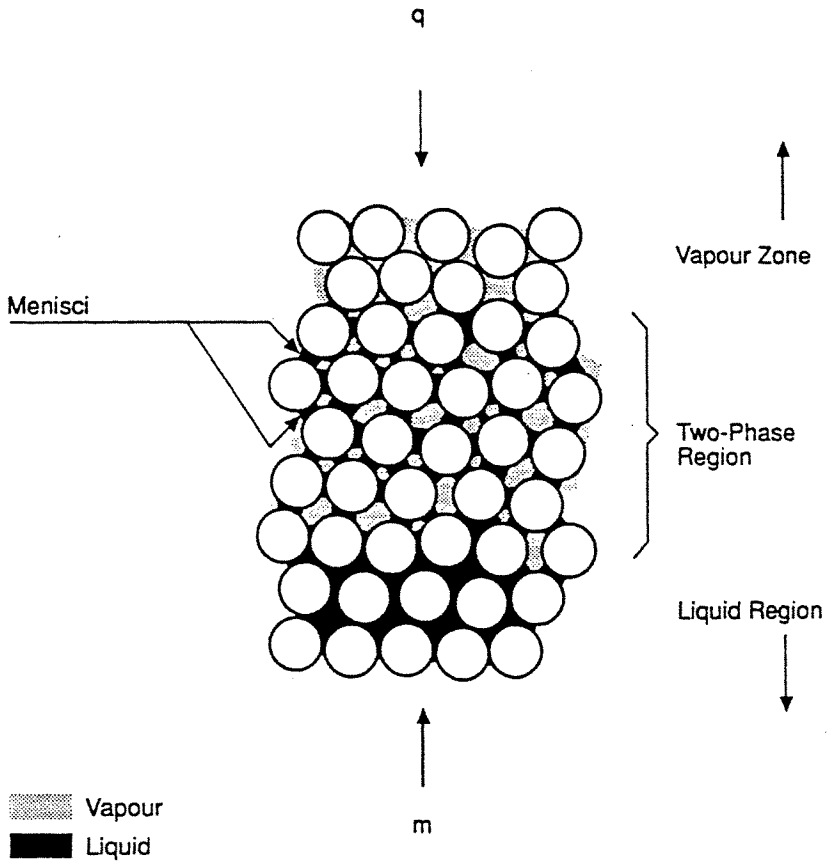

Figure 17. Physical model of two-phase region located between thin vapour zone and liquid region of wick: radii of voids are of the order of 10^{-5} m

Up to now, it has been assumed that the mass transfer by evaporation occurs on a plane interface which is located between the vapour zone and the liquid region of the wick structure. To explain the pumping process, it is now necessary to consider the interface from a microscopic point of view. The phase boundary surface is composed of the sum of the menisci surfaces that have been formed by wetting in an interfacial region or 'two-phase region' which is spatially expanded between the vapour zone and the liquid region. As an illustration, the two-phase region is sketched in Figure 17. A typical size of the menisci formed is about 10^{-5} m which corresponds to the pore size of the wick.

On the curved surface of a meniscus, there exists a pressure rise Δp_c which is known as 'capillary pressure'. Its value is proportional to the reciprocal value of the radius of curvature r' of the meniscus. r' is approximately equal to the effective pore radius $r_{p,eff}$:

$$\Delta p_c = \frac{2\sigma\cos\gamma}{r'} \simeq \frac{2\sigma\cos\gamma}{r_{p,eff}} \tag{6}$$

σ is the surface tension of the working fluid and γ is its contact angle.

In the steady-state condition, the capillary pressure rise Δp_c is in equilibrium with the sum of the internal pressure losses of the capillary pump, i.e. Δp_{int} plus the pressure loss in the loop, Δp_{loop}:

$$\Delta p_c = \Delta p_{int} + \Delta p_{loop} \tag{7}$$

In the steady-state working range, the effective capillary pumping pressure is equal to the pressure drop of the

loop. Hence equation (7) yields

$$\Delta p_{eff} = \Delta p_c - \Delta p_{int} \tag{8}$$

In order to predict the pumping limit curve, one has to calculate the sum of the internal pressure losses. Δp_{int} is composed of (see Figure 16)

(*a*) the flow losses $p_6 - p_7$ of the liquid working fluid in the feeder tubes and liquid channels of the wick structure between positions 6 and 7 in Figure 16
(*b*) the pressure loss $p_7 - p_8$ caused by the movement of the liquid working fluid in the liquid region of the wick structure between positions 7 and 8
(*c*) the pressure loss $p_1 - p_2$ caused by the vapour flow in the vapour zone of the wick structure between positions 1 and 2
(*d*) the flow losses $p_2 - p_3$ of the vapour in the grooved evaporation surface and in the vapour-collecting channels of the cover plate between positions 2 and 3.

The sum is written as

$$\Delta p_{int} = (p_6 - p_7) + (p_7 - p_8) + (p_1 - p_2) + (p_2 - p_3) \tag{9}$$

Figure 18, for example, shows the calculated pump limit curve of the capillary pump operated with the working fluid CCl_3F (freon R11). The fine dotted horizontal line presents the maximum available capillary pressure $\Delta p_{c\,max} = 2\sigma \cos \gamma / r'_{III}$; r'_{III} denotes the minimum meniscus radius. One obtains the pumping limit curve, if $\Delta p_{c\,max}$ is reduced by the sum of internal pressure losses, Δp_{int} as a function of the heat flux density q.

The calculation of the pressure losses of the liquid and the vapour flows in the wick structure was performed with the aid of a mathematical model which treats the associated heat and fluid flow in the porous wick [6,19].

Self-regulation of capillary pumping pressure

If the applied heat flux is increased, the mass flow of the working fluid and, consequently, the flow resistance in the capillary pump and in the loop increase. Since pressure equilibrium exists in the steady-state condition,

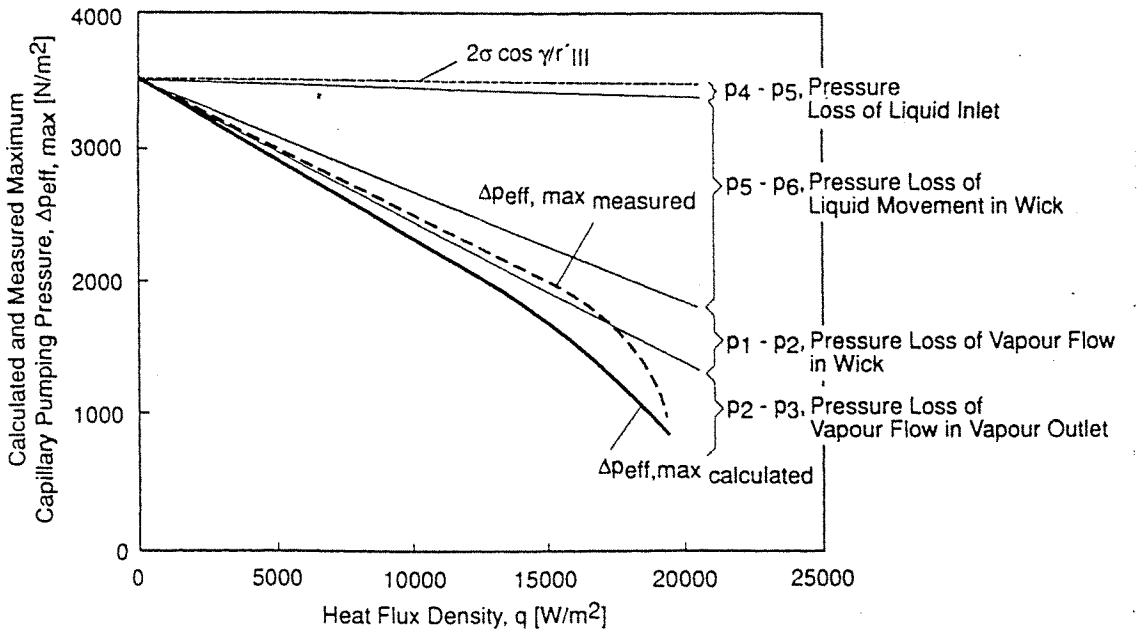

Figure 18. Calculated maximum effective capillary pumping pressure $\Delta p_{eff,max}$ against applied heat flux density

the capillary pressure adjusts in response to the variable pressure loss if the heat flux is changed. In the following, different working conditions are considered by which the selfregulation of the pumping pressure is qualitatively explained.

(*a*) *Nonoperative condition I*

In the nonoperative condition, the wick structure is completely filled with liquid. This is shown in Figure 19. No heat is applied; that means that no fluid transport occurs. In the performance diagram, Figure 9, this condition is marked by 'I'.

(*b*) *Steady-state working ranges II*

If a heat flux $Q_{min} \leqslant Q < Q_{dry}$ is applied to the capillary pump, liquid is displaced in the surface region of the wick, see Figure 20. A stable vapour zone is formed which shows a fixed interface or, in the microscopic view, a stationary thin two-phase region. Within the two-phase region, liquid and vapour coexist in the porous structure as illustrated in Figure 17.

During the circulation in the loop, the working fluid undergoes a total pressure loss Δp_{II}. This pressure loss is in equilibrium with the capillary pressure $\Delta p_{c,II} = 2\sigma \cos\gamma / r'_{II}$; r'_{II} denotes the radii of curvature of the menisci in the steady-state working range II. In the performance diagram in Figure 9, the steady-state working field extends below the pumping limit curve. The working points are located at the pump characteristic and at the flow resistance characteristic of the loop, respectively.

(*c*) *Pump limit III*

If the heat flux is increased to $Q_{III} \lesssim Q_{dry}$, the mass flow rises to m_{III} and the total pressure loss extends to Δp_{III}. The capillary pressure increases to $\Delta p_c = 2\sigma \cos\gamma / r'_{III}$ and the radius of curvature of the menisci decreases to r'_{III}. In the Figure 9, this condition is marked by 'III', which is located at the pumping limit curve.

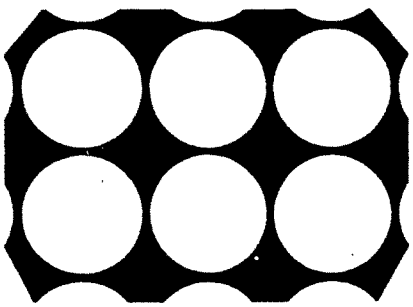

Figure 19. Porous structure of wick saturated with liquid working fluid in nonoperative condition I

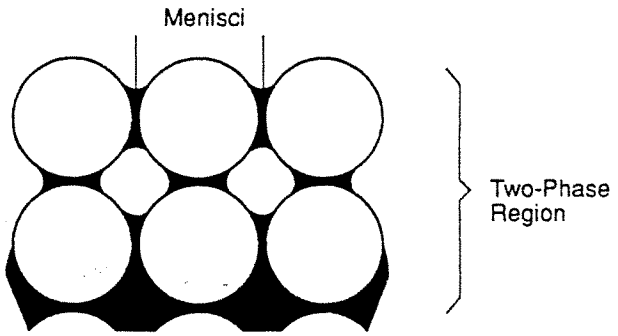

Figure 20. Menisci formed in two-phase region of wick in steady-state working range II

In the two-phase region, further liquid is displaced by the vapour. The three-phase line of the wetting working fluid withdraws to the equators of the spheres, as shown in Figure 21.

Summarizing, the self regulation of the mass flow in proportion to the applied heat flux is explained by the movement of the three-phase line of the menisci, that means that a progression or a withdrawal, respectively, of the three-phase line occurs in the case of a reduction or an increase of the applied heat flux. This is illustrated in Figure 22.

(d) Dry out IV

A dry out takes place, if the mass flow available by capillary pumping is smaller than that required for the transport of the heat, i.e. $Q_{IV} > Q_{III}$. In Figure 9, this condition is marked by 'IV'. The vapour zone now expands into the whole wick structure.

Boiling heat transfer in porous wick structure

The mass transfer by evaporation to the vapour phase takes place, if one regards the wick structure as packed spheres, from the surfaces of the menisci that have been formed between the spheres in the two-phase region. The voids that exist between the spheres are filled with vapour. This assumption was presented in Figure 17. For an explanation of the boiling heat transfer process at the surfaces of the menisci the 'model of the

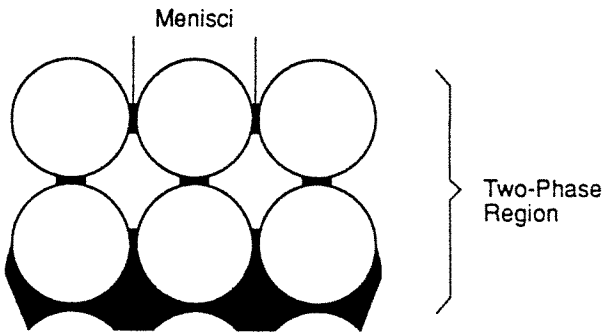

Figure 21. Menisci formed in two-phase region of wick at pumping limit III

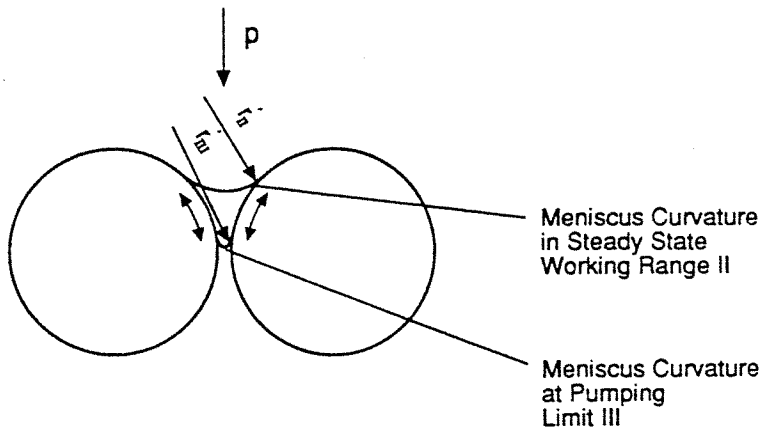

Figure 22. Variation of curvature radius of meniscus in two-phase region in response to a changing pressure drop of the loop in the steady-state working range and at pump limit

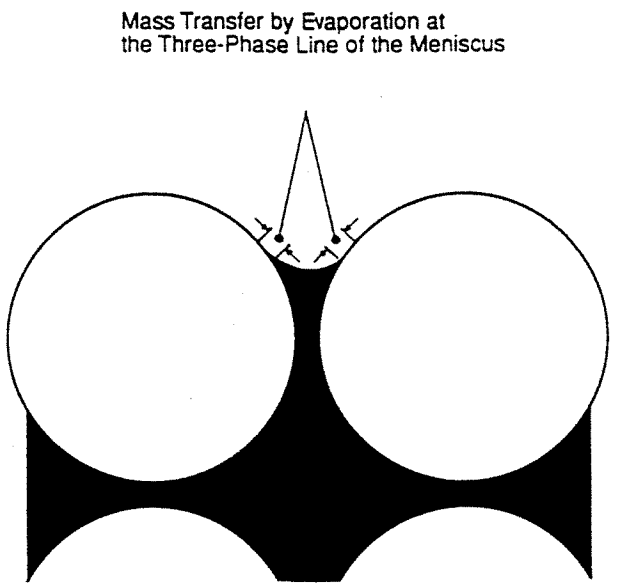

Figure 23. Boiling heat transfer of working fluid taking place at the interface and in the two-phase region, respectively, of the wick

evaporating meniscus is adopted [6]. In the literature, a number of publications can be found on the theoretical and experimental work on this topic, [7–12].

The small contact region of the menisci may be regarded as a wetting liquid film, of which the thickness decreases, see Figure 23. With respect to the studies which have been made in the field of a boiling curved surface, it is assumed that the mass transfer by evaporation takes place in a small region around the three-phase line called the evaporating thin film. The boiling heat transfer in the porous structure of the wick may therefore be regarded as a special case of the liquid film boiling with variable thickness in the region of the three-phase line. Thus it is assumed that the mass transfer by evaporation occurs from the surface of the liquid after the heat has flown across the film via conduction.

On the basis of this assumption, the evaporation of the working fluid occurs at a large number of menisci which have been formed in the two-phase region of the wick structure. At the three-phase line of the menisci, it has been suggested [12] that meniscus oscillations might occur owing to Marangoni convection, caused by local gradients of the surface tension. These arguments are considered to be the reason for the significant augmentation of the heat transfer in porous structures compared with the heat transfer at a plane heated surface. The nucleate boiling model, which is promoted by several authors [13–18] for the explanation of the boiling process in porous structures, cannot be adopted here for the description of the boiling heat transfer in the capillary pump.

OVERALL HEAT TRANSFER

The overall heat transfer coefficient h, which is plotted in Figures 11 and 12, can also be estimated. The reciprocal value of the heat transfer coefficient is composed of the sum of the thermal resistivity values from the individual heat transfer steps. The contact area between the grooved surface and the wick surface was chosen to be the heat transfer area.

$$\frac{1}{h} = \frac{s}{\lambda_{A1}} + \frac{1}{\alpha_1} + \frac{\delta}{\lambda_{por}} + \frac{1}{\alpha_2} \tag{11}$$

where

$\frac{s}{\lambda_{A1}}$ is the thermal resistivity as a result of heat conduction in the cover plate with thickness s from the heat input surface of the capillary pump to the grooved evaporation surface; λ_{A1} is the thermal conductivity of the cover plate material.

$\frac{1}{\alpha_1}$ thermal resistivity as a result of the heat transfer from the grooved surface to the wick surface; α_1 is the contact conductance heat transfer coefficient.

$\frac{\delta}{\lambda_{por}}$ is the thermal resistivity as a result of heat conduction in the vapour zone with thickness δ from the wick surface to the boiling meniscus surface; λ_{por} is the thermal conductivity of the porous wick.

$\frac{1}{\alpha_2}$ is the thermal resistivity as a result of the heat transfer of the boiling working fluid; α_2 is the heat transfer coefficient of the boiling working fluid.

The estimation of the values of the thermal resistivities clearly indicates that the heat conduction in the vapour zone is the rate-determining partial step of the overall heat transfer. For the example of the capillary pump described here, the term δ/λ_{por} is at least one order of magnitude higher than the values of the resistivities of the other partial steps. Referring to equation (11), one can then conclude that the reciprocal value of h is approximately equal to the term δ/λ_{por}.

One obtains a simple relation to calculate the overall heat transfer coefficient of a capillary pump:

$$h \simeq \frac{\lambda_{por}}{\delta} \tag{12}$$

The thickness δ of the vapour zone can be calculated with the aid of the mathematical model [6, 19]. It was found that δ was dependent on the geometrical size of the fins of the grooved surface, and that δ was independent of the heat flux density applied. This means that the vapour-zone thickness remains constant during the heat-flux change. On the assumption of a typical fin width x of 1 mm, thicknesses of $\delta = 0.1$ mm for the working fluid CCl_3F (R11) and $\delta = 0.014$ mm for ammonia have been calculated.

REFERENCES

1 Chalmers, D. R. (1987). Proceedings of 6th International Heat Pipe Conference, Grenoble, France.
2 Chalmers, D. R. *et al.* (1986). 4th Joint Thermophysics Heat Transfer Conference, Boston Paper AIAA-86-1295.
3 Wulz, H. G. (1988). Annual Congress of the Deutsche Gesellschaft für Luft-und Raumfahrt, Darmstadt, Yearbook p. 205.
4 Wulz, H. G. and Kreeb, H. European Patent EP 0 242 669 B1.
5 Wulz, H. G. and Kreeb, H. German Patent DE 3613802 C2.
6 Wulz, H. G. (1991). Doctoral thesis, Institute for Thermodynamics A, Technical University of Munich, Germany.
7 Derjaguin, B. V. and Zorin, Z. M. (1957). Proceedings of 2nd International Congress on Surface Activity (London), Vol. 2, pp. 145–162.
8 Potash, M. and Wayner, P. C. Jr. (1951). *Int. J. Heat Mass Transfer*, **15**, 1951.
9 Renk, F. J. and Wayner, P. C. Jr. (1979) *J. Heat Transfer*, **101**, 59.
10 Mirzamoghadam, A. and Catton, I. (1988). *J. Heat Transfer*, **110**, 201.
11 Renk, F. J. and Wayner, P. C. Jr. (1979) *J. Heat Transfer*, **101**, 55.
12 Mirzamoghadam, A. and Catton, I. (1988). *J. Heat Transfer*, **110**, 208.
13 Webb, R. L. (1983). *Heat Transfer Engineering*, **4**(3/4), 71–82.
14 Czikk, A. M. and O'Neill, P. S. (1979). *Advances in enhanced heat transfer*, ASME, NY, pp. 53–60.
15 Kim, C. J. and Bergles, A. E. (1985). HTL-36, ISU-ERI-Ames-86220, Iowa State University, Ames, AI, USA.
16 Bergles, A. E. and Chyu, M. C. (1982). *ASME J. Heat Transfer*, **104**, 279–285.
17 Konev, S. V. and Mitrovic, J. (1986). *Int. J. Heat Mass Transfer*, **29**(1), 91.
18 Nakayama, W. *et al.* (1980) *ASME J. Heat Transfer*, **102**, 445–456.
19 Wulz, H. G. and Embacher, E. (1990). 5th Joint Thermophysics and Heat Transfer Conference, Seattle WA., USA, Paper AIAA-90-1739.